

# New Closed-Form ASER Expressions for Dual-Hop Mixed THz-RF Cooperative Relay Networks

Soumendu Das, Nagendra Kumar, Dharmendra Dixit

**Abstract**—In this paper, we consider a dual-hop mixed THz-RF system model for backhaul-fronthaul applications where the link between source and destination is established only through the relay node in which decode-and-forward relaying protocol is used. The THz link suffers from the joint impact of antenna misalignment and stochastic characteristics of wireless channels, including the effect of environmental conditions such as pressure, humidity, and temperature. The envelope of THz link in the first hop follows a generalized  $\alpha - \mu$  distribution, and for the RF end, the Nakagami- $m$  distribution is considered. In this context, we obtain new closed-form expressions of the cumulative density function and the moment-generating function of the end-to-end signal-to-noise ratio. Further, we derive the average symbol error rate expressions for coherent rectangular quadrature amplitude modulation (RQAM) and coherent hexagonal QAM (HQAM), as well as the non-coherent modulation scheme. The asymptotic behavior is also discussed to examine the system's diversity. Furthermore, the impact of several parameters, such as fading coefficients of individual links and antenna misalignment, as well as the distance between nodes, are also highlighted in the system's performance. Moreover, Monte Carlo simulations are used to validate the presented analytical framework. Finally, the presented numerical insights aid in the extraction of practical design principles.

**Index Terms**—Terahertz, radio frequency, quadrature amplitude modulation,  $\alpha - \mu$  distribution, Nakagami- $m$  distribution, average symbol error rate, diversity order.

## I. INTRODUCTION

OVER the last few years, the number of wireless devices are increased at an expeditious rate and thus the significant accretion of wireless data traffic has encouraged the investigation of suitable regimes in the higher frequency bands of unused radio spectrum such as the terahertz (THz) band [1] to meet the escalating requirements of higher data rates with negligible latency. Unlicensed THz spectrum is cost-effective and theoretically competent to provide extremely high bandwidth [2], [3], [4] due to its existence in the higher region of the spectrum (0.1-10 THz) [5]. Thus, THz band is appropriate for wireless fiber extenders in backhaul link particularly when fiber optic link is burdensome to establish due to geographical challenges. Despite these advantages, the THz spectrum immensely suffers from severe attenuation due to molecular absorption [6]. When a signal with such a high frequency interacts with molecules of air medium, the energy of the signal is absorbed mostly due to the water vapor

molecules present in the atmosphere [7]. Generally,  $\alpha - \mu$  distribution is used to model THz communication link because of its versatile statistical behavior which includes several well-known channel models such as Rayleigh, Nakagami- $m$ , Weibull, Hoyt, Rice, Gamma, Chi-square, etc. [8].

### A. Related Literature

In literature, a novel THz band propagation model is discussed in [9]. In order to evaluate the performance of THz link, a path loss model due to molecular absorption in the 275 – 400 GHz band is considered in [10] and the channel capacity of THz link is calculated in [11]. Whereas, absorption loss due to components of propagation medium such as air, water, and natural gas is presented in [12]. Likewise in [13], authors have discussed a multi-ray THz model.

Performance of THz system can degrade severely due to hardware imperfections like in-phase and quadrature imbalance, minute misalignment of highly directional transceiver antennae [14], etc. Therefore, an extensive investigation is mandatory in modeling the particularities of THz channel as it is relatively new to explore. The impact of antenna misalignment is investigated in [15] and [16]. The influence of highly directive antennae in the THz band is studied in [15]. In [17], authors have investigated the joint impact of antenna misalignment and fading in THz-wireless systems in terms of outage probability and channel capacity.

A multipath model for THz channel is discussed in [18] and [19] considering Nakagami- $m$  fading distribution for line-of-sight as well as non-line-of-sight conditions and experimental results show the existence of shadowing in 300 GHz band [19]. As a consequence, THz spectrum is questionable for fronthaul due to its high sensitivity to blockage. Thus, the second hop is assumed to work in the RF spectrum.

Further to improve the quality of communication, various relaying schemes can be employed at the relay node such as decode-and-forward (DF), amplify-and-forward (AF), compress-and-forward (CF), etc. Although, AF is mostly preferred as it is cheap and the complexity of signal processing is very low. In spite of the complexity of decoding, DF can be used as relaying protocol due to its better performance than AF. In [20] and [21], authors have modeled a dual-hop THz system considering AF and DF relaying protocol, respectively, and checked its suitability for backhaul communications. In [22], authors have modeled a multihop system operating over THz frequency range while in [23], the performance of RF band relaying system is observed. In [24], authors have modeled a dual-hop mixed THz-RF model and

Soumendu Das and Nagendra Kumar are with the Department of Electronics and Communication Engineering, National Institute of Technology Janshedpur, Jharkhand-831014, India (e-mail: 2021rsec009@nitjsr.ac.in, kumar.nagendra86@gmail.com)

Dharmendra Dixit is with the Department of Electronics Engineering, Rajkiya Engineering College, Sonbhadra, U.P. India (ddixit@recsonbhadra.ac.in)

calculated average symbol error rate (ASER) expressions for differential binary phase shift keying (DBPSK),  $M$ -ary pulse amplitude modulation (PAM) and non-return-to-zero (NRZ) on-off keying (OOK) modulation schemes.

Further, limited bandwidth is optimally utilized to achieve enhancement in data rates by an adaptive selection of higher-order quadrature amplitude modulation (QAM) schemes such as rectangular QAM (RQAM) [25], squared QAM (SQAM) and hexagonal QAM (HQAM)[26]. Amongst these RQAM is the most flexible modulation scheme as it includes special cases such as SQAM, quadrature phase shift keying (QPSK), multi-level amplitude shift keying (M-ASK), and orthogonal binary frequency shift keying (OBFSK). It has a lot of applications such as asymmetric subscriber loops, high-speed mobile communication, etc. Several authors have discussed the performance of higher-order QAM schemes for several system and channel models [27], [28], [29], [30], [31], [32]. To the best of our knowledge, the ASER performance of practically useful QAM schemes for dual-hop mixed THz-RF cooperative relay networks is not explored yet.

### B. Motivations

With the move towards 6G and beyond wireless technologies, ultra-high data transmission rates, extremely large bandwidth, and very low latency are essential for multimedia transmission over wireless channels. 3rd generation partnership project (3GPP) Release-14 (LTE-advanced) and Release-15 (5G-New radio) have suggested the usage of higher order QAM, such as 256-QAM and 1024-QAM, for different high data rate applications [33]. Taking the above discussions into consideration, the mixed THz-RF based relay networks with QAM schemes become a potential technique to meet these demands. Although, in literature, dual-hop mixed THz-RF based cooperative relay networks have not been studied yet to analyze the ASER performance of practically important coherent QAM schemes. It motivates us to study and analyze the considered system, which will be of immense interest in 6G and beyond for the system designers.

### C. Contributions

For the THz wireless fiber extender system, we study a suitable and generalized system and channel model that takes into account many design factors as well as their interactions. In this paper, we consider a dual-hop mixed THz-RF based DF relay network considering  $\alpha - \mu$  and Nakagami- $m$  distribution for the THz and RF links, respectively. The main contributions of this manuscript are as follows:

- 1) We obtain a new closed-form expression for the cumulative density function (CDF) of the end-to-end signal-to-noise ratio (SNR).
- 2) A new moment-generating function (MGF) of end-to-end SNR is derived using the obtained CDF expression.
- 3) The generalized ASER expressions of coherent RQAM and HQAM schemes are obtained using the well-known CDF-based approach.

- 4) The generalized ASER expression of non-coherent FSK (NCFSK) is also obtained using the MGF-based approach.
- 5) In addition, the asymptotic expression of ASER for RQAM is presented.
- 6) The diversity order is obtained with the aid of the derived asymptotic ASER expression.

### D. Notations

Some notations that are used in the paper are as follows.  $\Gamma(\cdot)$  and  $\Gamma(\cdot, \cdot)$  represent the complete gamma function [34, eq. (8.310.1)] and upper incomplete gamma function [34, eq. (8.350.2)], respectively,  ${}_1F_1(\cdot; \cdot; \cdot)$  represents the confluent hypergeometric function of first kind [34, eq. (9.210.1)],  ${}_pF_q(a_1, \dots, a_p; b_1, \dots, b_q; z)$  represents generalized hypergeometric function [35, eq. (7.2.3)],  $\binom{\cdot}{\cdot}$  represents the binomial coefficient,  $G_{p,q}^{m,n} \left[ z \begin{matrix} a_1, \dots, a_p \\ b_1, \dots, b_q \end{matrix} \right]$  represents the Meijer-G function [34, eq. (9.301)], and Fox-H function [36, eq. (17)] is represented by  $H_{p,q}^{m,n} \left[ z \begin{matrix} (a_1, A_1), \dots, (a_p, A_p) \\ (b_1, B_1), \dots, (b_q, B_q) \end{matrix} \right]$ . Further, multivariate Fox-H function [37, eq. (A.1)] can be expressed as

$$H_{p,q;p_1,q_1;\dots;p_r,q_r}^{0,n;m_1,n_1;\dots;m_r,n_r} \left[ z \begin{matrix} z_1 \\ \vdots \\ z_r \end{matrix} \begin{matrix} (a; \alpha_1, \dots, \alpha_r)_{1:p} : (c, \gamma)_{1:p_1} ; \dots ; (c, \gamma)_{1:p_r} \\ (b; \beta_1, \dots, \beta_r)_{1:q} : (d, \delta)_{1:q_1} ; \dots ; (d, \delta)_{1:q_r} \end{matrix} \right].$$

### E. Organization of the paper

The rest of the paper is organized as follows: In Section II, we discuss the system and channel model of relay assisted THz-RF system. In Section III, we analyze the performance of the proposed system model. In subsections III-A, the expression for the CDF of end-to-end SNR is presented. In III-B, a new closed-form expression for the MGF of end-to-end SNR is derived. In subsection III-C, ASER expressions for coherent QAM schemes and non-coherent FSK modulation schemes are derived. Moreover, asymptotic analysis of RQAM modulation scheme is also presented in subsection III-D. In Section IV, simulation and theoretical results are compared. Finally, the paper is concluded in Section V.

## II. SYSTEM AND CHANNEL MODEL

### A. System model

We consider a dual-hop mixed THz-RF wireless system model consisting of a source node (S), a destination node (D), and a relay node (R), as shown in Fig. 1. It is assumed that the direct link between S and D is extremely weak, so it can be neglected. Therefore, the communication link between S and D is established through R only, where it uses DF relaying technique. Therefore, the overall downlink communication is accomplished in two-time slots. In the first time slot, the symbol is transmitted from S through the S-R channel and received by R. In the next time slot, R decodes the received symbol. If the symbol is found to be correct, the relay re-encodes the symbol to transmit it over R-D link. Finally, D decodes the symbol from the received signal.

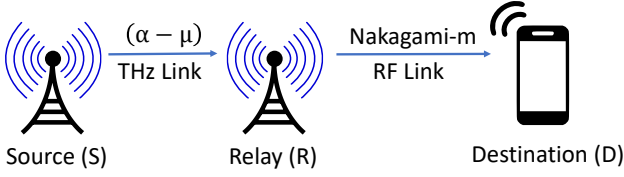


Fig. 1. THz-RF System Model

## B. Channel model

1) *THz link (hop 1)*: In the first hop, symbols are transmitted from S over the S-R link. Thus, the signal received by R can be mathematically expressed as

$$y_r = \sqrt{P_s} h_{sr} x_s + w_r, \quad (1)$$

where  $P_s$  is the power of the signal transmitted from S,  $h_{sr}$  is the channel coefficient of S-R link,  $x_s$  is the transmitted symbol having unit energy, and  $w_r$  is the additive white Gaussian noise (AWGN) with zero mean and variance  $N_1$ . Further, the channel coefficient  $h_{sr}$  can be represented as

$$h_{sr} = h_{d1} h_{a1} h_{f1} h_{p1}, \quad (2)$$

where  $h_{d1}$  represents the deterministic free space path-loss which can be defined using Friis equation[38] as

$$h_{d1} = \frac{c\sqrt{G_{ts}G_{rr}}}{4\pi f_{sr}} d_{sr}^{-(0.5\eta_1)}, \quad (3)$$

wherein  $c$  is the speed of light in free space,  $f_{sr}$  is the frequency of the signal transmitted by S,  $d_{sr}$  is the distance between S and R,  $G_{ts}$  is the transmitter antenna gain of node S and  $G_{rr}$  is the receiver antenna gain of node R. For free space or air medium without shadowing, path loss exponent  $\eta_1$  is considered to be 2. The value of  $\eta_1$  increases in urban regions, and if shadowing is present due to a large factory or high-rise buildings,  $\eta_1$  increases further.

The deterministic loss due to atmospheric molecular absorption,  $h_{a1}$ , in THz frequency range is modeled by using Buck's equation [39] as

$$h_{a1} = \exp[-0.5\kappa_\alpha(f_{sr}, T, P, \psi)d_{sr}], \quad (4)$$

where  $\kappa_\alpha$  is the absorption coefficient [24, eq. (8)] and it depends on atmospheric parameters like absolute temperature (T), pressure (P), and relative humidity ( $\psi$ ) present in the air.

The envelope of multipath fading  $h_{f1}$  in THz link is assumed to follow generalized  $\alpha - \mu$  distribution described by fading parameter,  $\alpha$  ( $\alpha > 0$ ),  $\alpha$ -root mean value,  $\Omega$ , and the normalized variance,  $\mu$  ( $\mu \geq \frac{1}{2}$ ), of the fading channel envelope. The probability density function (PDF) of  $h_{f1}$  is represented with the aid of [8, eq. (1)] as

$$f_{h_{f1}}(x) = \frac{\alpha\mu^\mu x^{\alpha\mu-1}}{\Omega^{\alpha\mu} \Gamma(\mu)} \exp\left(-\frac{\mu x^\alpha}{\Omega^\alpha}\right). \quad (5)$$

Whereas, the CDF expression of  $h_{f1}$  is obtained by integrating (5) with the aid of [40, eq. (4.1)] and further, the integration can be expressed in terms of upper incomplete gamma function [34, eq. (8.352.2)] as

$$F_{h_{f1}}(x) = 1 - \frac{1}{\Gamma(\mu)} \Gamma\left(\mu, \frac{\mu x^\alpha}{\Omega^\alpha}\right). \quad (6)$$

Further,  $h_{p1}$  represents the fading coefficient of pointing error due to antenna misalignment between S and R. Thus, it can be modeled as [41].

$$f_{h_{p1}}(x) = \frac{\phi x^{\phi-1}}{S_0^\phi}, \quad 0 \leq x \leq S_0 \quad (7)$$

where  $S_0$  is the fraction of power collected at the receiver when transmitter and receiver antennas are fully aligned, and  $\phi$  is the ratio of the square of equivalent beam radius  $w_{zeq}$  and standard deviation of pointing error displacement at the receiver  $\sigma_s^2$ . The value of  $S_0$  and  $\phi$  can be calculated as,  $S_0 = [erf(\nu)]^2$  and  $\phi = \frac{w_{zeq}^2}{4\sigma_s^2}$ , where,  $\nu$  and  $w_{zeq}$  are calculated from the radius of the detector aperture and beam footprint radius  $w_z$  at a transmission distance  $z$  as mentioned in [41, (9)]. We consider  $h_1 = h_{f1} h_{p1}$ , thus, the PDF of  $h_1$  can be evaluated with the aid of [40] as

$$f_{h_1}(x) = \left[ \frac{\phi \mu \left(\frac{\phi}{\alpha}\right) x^{(\phi-1)}}{(\Omega S_0)^\phi \Gamma(\mu)} \right] \Gamma\left(\frac{\alpha\mu - \phi}{\alpha}, \frac{\mu x^\alpha}{(\Omega S_0)^\alpha}\right). \quad (8)$$

The CDF of  $h_1$  can be calculated using (6) and (7) with the aid of [40] as expressed in (9). The calculation of (9) is elaborated in subsection A of the appendix.

$$F_{h_1}(x) = 1 - \frac{1}{\Gamma(\mu)} \frac{\phi}{\alpha} G_{2,3}^{3,0} \left[ \frac{\mu x^\alpha}{\Omega^\alpha S_0^\alpha} \middle| \begin{matrix} 1, \frac{\phi}{\alpha} + 1 \\ \mu, 0, \frac{\phi}{\alpha} \end{matrix} \right], \quad (9)$$

2) *RF link (hop 2)*: In the DF relaying technique, node R decodes the received symbol of the first time slot. If the received symbol is found to be error-free, node R re-encodes the decoded symbol and transmits it through R-D link in the second time slot. The received signal at the destination can be expressed as

$$y_d = \sqrt{P_r} h_{rd} \tilde{x}_r + w_d, \quad (10)$$

where  $\tilde{x}_r$  and  $P_r$  are the re-encoded unit energy symbol transmitted from R and transmitted power at R, respectively.  $h_{rd}$  is the channel coefficient of the second hop.  $w_d$  is the AWGN with zero mean and variance  $N_2$ . In case of incorrect reception at R, no symbol is transmitted further. Also, similar to THz link,  $h_{rd}$  can be represented in the form of deterministic free space path gain,  $h_{d2}$ , and fading channel coefficient,  $h_{f2}$ , as

$$h_{rd} = h_{d2} h_{f2}, \quad (11)$$

where the deterministic coefficient for free space path-loss,  $h_{d2}$ , can be modeled similar to (3) as

$$h_{d2} = \frac{c\sqrt{G_{tr}G_{rd}}}{4\pi f_{rd}} d_{rd}^{-(0.5\eta_1)}, \quad (12)$$

where  $G_{tr}$  is the transmitter antenna gain of node R and  $G_{rd}$  is the receiver antenna gain of node D.  $f_{rd}$  and  $d_{rd}$  are the

frequency of the signal used in RF link and the distance it between nodes R and D, respectively. The envelope of  $h_{f_2}$  is assumed to follow the Nakagami- $m$  distribution. Thus, the PDF, and the CDF expressions of  $h_{f_2}$ , can be given as, respectively [42]

$$f_{h_{f_2}}(x) = \frac{2m^m x^{2m-1}}{(\Omega_m)^m \Gamma(m)} \exp\left(-\frac{m}{\Omega_m} x^2\right), \quad (13)$$

$$F_{h_{f_2}}(x) = 1 - \frac{1}{\Gamma(m)} \Gamma\left(m, \frac{m}{\Omega_m} x^2\right), \quad (14)$$

where  $m$  is shape parameter and  $\Omega_m$  represents spread controlling parameter ( $m \geq \frac{1}{2}$ ,  $\Omega_m > 0$ ).

### III. PERFORMANCE ANALYSIS

In this section, we present the performance analysis of the considered system. In subsection III-A, a new expression for the CDF of end-to-end SNR is presented. In subsection III-B, a new closed-form for the MGF of end-to-end SNR is derived. The new generalized ASER expressions for coherent RQAM and HQAM schemes as well as non-coherent  $M$ -ary NCFSK scheme, are derived in subsection III-C. In subsection III-D, the asymptotic ASER expression for RQAM scheme and diversity order are given.

#### A. CDF expression for end-to-end SNR

At node R, DF relaying protocol is used, thus, end-to-end SNR,  $\lambda_e$ , of the mixed THz-RF link can be written as

$$\lambda_e = \min(\lambda_1, \lambda_2), \quad (15)$$

where  $\lambda_1$  and  $\lambda_2$  are the instantaneous SNRs of S-R (THz) and R-D (RF) links, respectively, which can be expressed as

$$\lambda_1 = |h_{sr}|^2 \frac{P_s}{N_1} = \frac{|h_{d1}|^2 |h_{a1}|^2 |h_{f1}|^2 |h_{p1}|^2 P_s}{N_1}, \quad (16)$$

$$\lambda_2 = |h_{rd}|^2 \frac{P_r}{N_2} = \frac{|h_{d2}|^2 |h_{f2}|^2 P_r}{N_2}. \quad (17)$$

We assume that the noise variances are same for both the nodes i.e. ( $N_1 = N_2$ ). Therefore, we define the average transmit SNR as  $\bar{\lambda}_0 = \frac{P_s}{N_1} = \frac{P_r}{N_2}$ . Further, the CDF expression for  $\lambda_e$  can be written as

$$F_{\lambda_e}(\lambda) = F_{\lambda_1}(\lambda) + F_{\lambda_2}(\lambda) - F_{\lambda_1}(\lambda)F_{\lambda_2}(\lambda), \quad (18)$$

where  $F_{\lambda_1}(\lambda)$  and  $F_{\lambda_2}(\lambda)$  are the CDF expressions of  $\lambda_1$  and  $\lambda_2$ , respectively and can be obtained with the aid of [40, eq. (5.4)]. The CDF of instantaneous SNR of THz link can be expressed using (9) as in (19).

$$F_{\lambda_1}(\lambda) = 1 - \frac{1}{\Gamma(\mu)} \frac{\phi}{\alpha} G_{2,3}^{3,0} \left[ \mu (\mathcal{A}\lambda)^{\alpha/2} \left| \begin{matrix} 1, \frac{\phi}{\alpha} + 1 \\ \mu, 0, \frac{\phi}{\alpha} \end{matrix} \right. \right], \quad (19)$$

where  $\mathcal{A} = \frac{N_1}{P_s |h_{d1}|^2 |h_{a1}|^2 \Omega_m^2 S_0^2}$ . The CDF expression of instantaneous SNR of RF link,  $\lambda_2$ , can be expressed as

$$F_{\lambda_2}(\lambda) = 1 - \frac{\Gamma(m, \mathcal{C}\lambda)}{\Gamma(m)}, \quad (20)$$

where  $\mathcal{C} = \frac{mN_2}{P_r |h_{d2}|^2 \Omega_m}$ . Thus, by substituting (19) and (20) into (18) and after simplification, we can obtain the CDF expression of end-to-end SNR,  $\lambda_e$ , as

$$F_{\lambda_e}(\lambda) = 1 - \mathcal{B} G_{2,3}^{3,0} \left[ \mu (\mathcal{A}\lambda)^{\alpha/2} \left| \begin{matrix} 1, \frac{\phi}{\alpha} + 1 \\ \mu, 0, \frac{\phi}{\alpha} \end{matrix} \right. \right] \Gamma(m, \mathcal{C}\lambda), \quad (21)$$

where the constant term  $\mathcal{B} = \frac{1}{\Gamma(\mu)\Gamma(m)} \frac{\phi}{\alpha}$ .

#### B. MGF expression of end-to-end SNR

We can evaluate MGF expression of end-to-end SNR,  $\lambda_e$ , with the aid of CDF-based approach as [28, eq. (6)]

$$\mathcal{M}_{\lambda_e}(s) = \int_{\lambda=0}^{\infty} s e^{-s\lambda} F_{\lambda_e}(\lambda) d\lambda, \quad (22)$$

where  $s$  is the Laplace variable. Further, substituting (21) into (22), the MGF expression can be written as

$$\mathcal{M}_{\lambda_e}(s) = s\mathcal{I}_1(0, s) - s\mathcal{B}\mathcal{I}_2(0, s), \quad (23)$$

where,

$$\mathcal{I}_1(\chi_1, \chi_2) = \int_{\lambda=0}^{\infty} \lambda^{\chi_1} e^{-\chi_2 \lambda} d\lambda, \quad (24)$$

and

$$\begin{aligned} \mathcal{I}_2(\chi_1, \chi_2) &= \int_{\lambda=0}^{\infty} \frac{\lambda^{\chi_1} \Gamma(m, \mathcal{C}\lambda)}{e^{\chi_2 \lambda}} G_{2,3}^{3,0} \left[ \mu (\mathcal{A}\lambda)^{\alpha/2} \left| \begin{matrix} 1, \frac{\phi}{\alpha} + 1 \\ \mu, 0, \frac{\phi}{\alpha} \end{matrix} \right. \right] d\lambda. \end{aligned} \quad (25)$$

A solution for both  $\mathcal{I}_1(\cdot, \cdot)$  and  $\mathcal{I}_2(\cdot, \cdot)$  integrations are given in subsection B and subsection C of the appendix, respectively. Substituting the results of  $\mathcal{I}_1(\cdot, \cdot)$  and  $\mathcal{I}_2(\cdot, \cdot)$  into (23) and after simplification, the MGF expression of  $\lambda_e$  can be expressed as

$$\mathcal{M}_{\lambda_e}(s) = 1 - \mathcal{B} H_{1,0:2,3;1,2}^{0,1:3,0;2,0} \left[ \begin{matrix} \mu \left( \sqrt{\frac{\mathcal{A}}{s}} \right)^{\alpha} \\ \frac{\mathcal{C}}{s} \end{matrix} \left| \begin{matrix} \nu_{\mathcal{M}} : \nu_2; \nu_3 \\ - : \nu_4; \nu_5 \end{matrix} \right. \right], \quad (26)$$

where,  $\nu_{\mathcal{M}}$  can be expressed as  $\nu_{\mathcal{M}} = \nu_1(0) = \left\{ \left(0; \frac{\alpha}{2}, 1\right) \right\}$ . The values of  $\nu_1$  to  $\nu_5$  are defined in subsection C of the appendix.

#### C. Exact ASER expressions

The well known CDF-based approach can be used to evaluate ASER expression of any modulation scheme in a communication system as [43, eq. (5)]

$$\mathcal{P}_s(e) = - \int_{\lambda=0}^{\infty} \mathcal{P}'_s(e|\lambda) F_{\lambda_e}(\lambda) d\lambda, \quad (27)$$

where  $\mathcal{P}'_s(e|\lambda)$  represents the first order derivative of conditional symbol error rate (SER) expression  $\mathcal{P}_s(e|\lambda)$  related to the particular modulation scheme and  $F_{\lambda_e}(\lambda)$  is the CDF expression for end-to-end SNR,  $\lambda_e$ , of the considered system.

1) *Coherent RQAM scheme*: The first order derivative of conditional SER expression for  $M = M_I \times M_Q$ -ary coherent RQAM modulation scheme is expressed as [29, eq. (4)]

$$\begin{aligned} \mathcal{P}_s^R(e | \lambda) &= \frac{1}{\sqrt{\lambda}} \left[ \mathcal{D} e^{-(0.5\lambda a^2)} + \mathcal{F} e^{-(0.5\lambda b^2)} \right] \\ &\quad - \frac{\mathcal{G}}{\sqrt{\pi}} e^{-\frac{\lambda}{2}(a^2+b^2)} {}_1F_1\left(1; 1.5; 0.5\lambda a^2\right) \\ &\quad - \frac{\mathcal{G}}{\sqrt{\pi}} e^{-\frac{\lambda}{2}(a^2+b^2)} {}_1F_1\left(1; 1.5; 0.5\lambda b^2\right), \end{aligned} \quad (28)$$

where  $\mathcal{D} = \frac{ap(q-1)}{\sqrt{2\pi}}$ ,  $\mathcal{F} = \frac{b(p-1)q}{\sqrt{2\pi}}$ ,  $\mathcal{G} = \frac{abpq}{\sqrt{\pi}}$ , wherein  $p = 1 - \frac{1}{M_I}$ ,  $q = 1 - \frac{1}{M_Q}$ ,  $a = \sqrt{\frac{6}{(M_I^2-1)+(M_Q^2-1)\beta^2}}$ ,  $b = \beta a$ .  $M_I$  is number of in-phase constellation points and  $M_Q$  is the number of quadrature-phase constellation points.  $\beta$  is the ratio of in-phase and quadrature-phase decision distances. Further, the generalized ASER expression of coherent RQAM can be obtained by putting (21) and (28) into (27) as

$$\begin{aligned} \mathcal{P}_s^R(e) &= -\mathcal{D}\mathcal{I}_1\left(-\frac{1}{2}, \frac{a^2}{2}\right) - \mathcal{F}\mathcal{I}_1\left(-\frac{1}{2}, \frac{b^2}{2}\right) \\ &\quad + \frac{\mathcal{G}}{\sqrt{\pi}} \left\{ \mathcal{I}_3\left(0, \frac{a^2+b^2}{2}, \frac{a^2}{2}\right) + \mathcal{I}_3\left(0, \frac{a^2+b^2}{2}, \frac{b^2}{2}\right) \right\} \\ &\quad + \mathcal{B}\mathcal{D}\mathcal{I}_2\left(-\frac{1}{2}, \frac{a^2}{2}\right) + \mathcal{B}\mathcal{F}\mathcal{I}_2\left(-\frac{1}{2}, \frac{b^2}{2}\right) \\ &\quad - \frac{\mathcal{B}\mathcal{G}}{\sqrt{\pi}} \left\{ \mathcal{I}_4\left(\frac{a^2+b^2}{2}, \frac{a^2}{2}\right) + \mathcal{I}_4\left(\frac{a^2+b^2}{2}, \frac{b^2}{2}\right) \right\}, \end{aligned} \quad (29)$$

where,

$$\mathcal{I}_3(\chi_1, \chi_2, \chi_3) = \int_{\lambda=0}^{\infty} \frac{\lambda \chi_1}{e^{\chi_2 \lambda}} {}_1F_1\left(1; \frac{3}{2}; \chi_3 \lambda\right) d\lambda, \quad (30)$$

and

$$\begin{aligned} \mathcal{I}_4(\chi_1, \chi_2) &= \int_{\lambda=0}^{\infty} e^{-\chi_1 \lambda} G_{2,3}^{3,0} \left[ \mu (\mathcal{A}\lambda)^{\alpha/2} \left| \begin{matrix} 1, \frac{\phi}{\alpha} + 1 \\ \mu, 0, \frac{\phi}{\alpha} \end{matrix} \right. \right] \\ &\quad \times \Gamma(m, \mathcal{C}\lambda) {}_1F_1\left(1; \frac{3}{2}; \chi_2 \lambda\right) d\lambda. \end{aligned} \quad (31)$$

A solution for  $\mathcal{I}_1(\cdot, \cdot)$ ,  $\mathcal{I}_3(\cdot, \cdot, \cdot)$ ,  $\mathcal{I}_2(\cdot, \cdot)$  and  $\mathcal{I}_4(\cdot, \cdot)$  are provided in Appendix. With the aid of solutions of  $\mathcal{I}_1(\cdot, \cdot)$ ,  $\mathcal{I}_3(\cdot, \cdot, \cdot)$ ,  $\mathcal{I}_2(\cdot, \cdot)$  and  $\mathcal{I}_4(\cdot, \cdot)$ , the generalized ASER expression for coherent RQAM modulation scheme is presented in (34) in terms of  $\Psi_1(\cdot)$  and  $\Psi_2(\cdot, \cdot)$  function. Where,  $\Psi_1(\cdot)$  and  $\Psi_2(\cdot, \cdot)$  are represented in (32) and (33) respectively.

$$\Psi_1(\chi) = H_{1,0:1,3,0;2,0}^{0,1:3,0;2,0} \left[ \begin{matrix} \mu \left(\frac{2\mathcal{A}}{\chi}\right)^{\frac{\alpha}{2}} \\ \frac{2\mathcal{C}}{\chi} \end{matrix} \left| \begin{matrix} \nu_{\mathcal{R}} : \nu_2; \nu_3 \\ - : \nu_4; \nu_5 \end{matrix} \right. \right], \quad (32)$$

where  $\nu_{\mathcal{R}}$  can be expressed as  $\nu_{\mathcal{R}} = \nu_1 \left(-\frac{1}{2}\right) = \left\{\left(\frac{1}{2}; \frac{\alpha}{2}, 1\right)\right\}$ .

$$\begin{aligned} \Psi_2(\chi_1, \chi_2) &= \frac{1}{\chi_2} H_{1,0:1,2;2,3;1,2}^{0,1:1,0;3,0;2,0} \left[ \begin{matrix} \left(\frac{\chi_1}{\chi_2}\right) \\ \mu \left(\frac{2\mathcal{A}}{\chi_2}\right)^{\alpha/2} \\ \left(\frac{2\mathcal{C}}{\chi_2}\right) \end{matrix} \left| \begin{matrix} \nu_6 : \nu_7; \nu_2; \nu_3 \\ - : \nu_8; \nu_4; \nu_5 \end{matrix} \right. \right], \end{aligned} \quad (33)$$

where,  $\nu_6$  to  $\nu_8$  are mentioned in subsection E of the appendix. It is well known that SQAM is a special case of RQAM when in-phase and quadrature-phase components are equal to  $\sqrt{M}$ . Thus, we can obtain an ASER expression for SQAM by putting  $M_I = M_Q = \sqrt{M}$  in (34). We can also get the average bit error rate (ABER) expression of BPSK scheme from (34) as a special case of RQAM by putting  $M_I = 2$ ,  $M_Q = 1$ ,  $p = 0.5$ ,  $q = 0$ ,  $a = \sqrt{2}$  and  $\beta = 0$ .

2) *Coherent HQAM scheme*: The first order derivative of conditional SER of  $M$ -ary HQAM scheme can be defined as [43, eq. (6)]

$$\begin{aligned} \mathcal{P}_s^H(e | \lambda) &= \sqrt{\frac{\alpha_h}{2\pi\lambda}} \left(\frac{B_c - B}{2}\right) e^{-(\frac{\alpha_h}{2}\lambda)} - \sqrt{\frac{\alpha_h}{3\pi\lambda}} \left(\frac{B_c}{3}\right) \\ &\quad \times e^{-(\frac{\alpha_h}{3}\lambda)} + \sqrt{\frac{\alpha_h}{6\pi\lambda}} \left(\frac{B_c}{2}\right) e^{-(\frac{\alpha_h}{6}\lambda)} \\ &\quad + \frac{2B_c\alpha_h}{9\pi} {}_1F_1\left(1; \frac{3}{2}; \frac{\alpha_h}{3}\lambda\right) e^{-(\frac{2\alpha_h}{3}\lambda)} \\ &\quad - \frac{B_c\alpha_h}{2\sqrt{3}\pi} \left[ {}_1F_1\left(1; \frac{3}{2}; \frac{\alpha_h}{2}\lambda\right) \right. \\ &\quad \left. + {}_1F_1\left(1; \frac{3}{2}; \frac{\alpha_h}{6}\lambda\right) \right] e^{-(\frac{2\alpha_h}{3}\lambda)}, \end{aligned} \quad (35)$$

where  $B$ ,  $B_c$ ,  $\alpha_h$  are different modulation parameters as defined in [44, Table-I] in terms of  $\tau$ ,  $\tau_c$  and  $K$ , respectively. Similar to RQAM, the ASER for HQAM scheme can be evaluated by putting (21) and (35) into (27) as

$$\begin{aligned} \mathcal{P}_s^H(e) &= \left(\frac{B - B_c}{2}\right) \sqrt{\frac{\alpha_h}{2\pi}} \mathcal{I}_1\left(-\frac{1}{2}, \frac{\alpha_h}{2}\right) \\ &\quad + \frac{B_c}{3} \sqrt{\frac{\alpha_h}{3\pi}} \mathcal{I}_1\left(-\frac{1}{2}, \frac{\alpha_h}{3}\right) - \frac{B_c}{2} \sqrt{\frac{\alpha_h}{6\pi}} \mathcal{I}_1\left(-\frac{1}{2}, \frac{\alpha_h}{6}\right) \\ &\quad + \frac{B_c\alpha_h}{2\sqrt{3}\pi} \left\{ \mathcal{I}_3\left(0, \frac{2\alpha_h}{3}, \frac{\alpha_h}{2}\right) + \mathcal{I}_3\left(0, \frac{2\alpha_h}{3}, \frac{\alpha_h}{6}\right) \right\} \\ &\quad - \frac{2B_c\alpha_h}{9\pi} \mathcal{I}_3\left(0, \frac{2\alpha_h}{3}, \frac{\alpha_h}{3}\right) + \mathcal{B} \left[ \sqrt{\frac{\alpha_h}{2\pi}} \left(\frac{B_c - B}{2}\right) \right. \\ &\quad \times \mathcal{I}_2\left(-\frac{1}{2}, \frac{\alpha_h}{2}\right) - \sqrt{\frac{\alpha_h}{3\pi}} \left(\frac{B_c}{3}\right) \mathcal{I}_2\left(-\frac{1}{2}, \frac{\alpha_h}{3}\right) \\ &\quad \left. + \sqrt{\frac{\alpha_h}{6\pi}} \left(\frac{B_c}{2}\right) \mathcal{I}_2\left(-\frac{1}{2}, \frac{\alpha_h}{6}\right) + \frac{2B_c\alpha_h}{9\pi} \mathcal{I}_4\left(\frac{2\alpha_h}{3}, \frac{\alpha_h}{3}\right) \right. \\ &\quad \left. - \frac{B_c\alpha_h}{2\sqrt{3}\pi} \left\{ \mathcal{I}_4\left(\frac{2\alpha_h}{3}, \frac{\alpha_h}{2}\right) + \mathcal{I}_4\left(\frac{2\alpha_h}{3}, \frac{\alpha_h}{6}\right) \right\} \right]. \end{aligned} \quad (36)$$

Note that a solution for  $\mathcal{I}_1(\cdot, \cdot)$ ,  $\mathcal{I}_3(\cdot, \cdot, \cdot)$ ,  $\mathcal{I}_2(\cdot, \cdot)$  and  $\mathcal{I}_4(\cdot, \cdot)$  are provided in Appendix. Using the solutions of  $\mathcal{I}_1(\cdot, \cdot)$ ,

$$\begin{aligned} \mathcal{P}_s^R(e) = & (p+q-2pq) + \frac{2\mathcal{G}}{\sqrt{\pi}} \frac{1}{(a^2+b^2)} \left[ {}_2F_1\left(1, 1; \frac{3}{2}; \frac{a^2}{a^2+b^2}\right) + {}_2F_1\left(1, 1; \frac{3}{2}; \frac{b^2}{a^2+b^2}\right) \right] + \frac{\mathcal{B}p(q-1)}{\sqrt{\pi}} \Psi_1(a^2) \\ & + \frac{\mathcal{B}(p-1)q}{\sqrt{\pi}} \Psi_1(b^2) - \frac{\mathcal{B}\mathcal{G}}{\sqrt{\pi}} \Psi_2(a^2, b^2) - \frac{\mathcal{B}\mathcal{G}}{\sqrt{\pi}} \Psi_2(b^2, a^2) \end{aligned} \quad (34)$$

$\mathcal{I}_3(\cdot, \cdot, \cdot)$ ,  $\mathcal{I}_2(\cdot, \cdot)$  and  $\mathcal{I}_4(\cdot, \cdot)$ , the ASER expression of generalized HQAM scheme can be expressed in terms of  $\Psi_3(\cdot)$  and  $\Psi_4(\cdot, \cdot)$  functions as represented in (39). Where the functions  $\Psi_3(\cdot)$  and  $\Psi_4(\cdot, \cdot)$  are represented in (37) and (38) respectively.

$$\Psi_3(\chi) = H_{1,0:2,3;1,2}^{0,1:3,0;2,0} \left[ \begin{array}{c} \mu \left( \frac{\mathcal{A}\chi}{\alpha_h} \right)^{\frac{\alpha}{2}} \\ \frac{\mathcal{C}\chi}{\alpha_h} \end{array} \middle| \begin{array}{l} \nu_{\mathcal{H}} : \nu_2; \nu_3 \\ - : \nu_4; \nu_5 \end{array} \right], \quad (37)$$

where  $\nu_{\mathcal{H}}$  can be expressed as  $\nu_{\mathcal{H}} = \nu_1 \left(-\frac{1}{2}\right) = \left\{ \left(\frac{1}{2}; \frac{\alpha}{2}, 1\right) \right\}$ .

$$\begin{aligned} & \Psi_4(\chi_1, \chi_2) \\ = & H_{1,0:1,2;2,3;1,2}^{0,1:1,0;3,0;2,0} \left[ \begin{array}{c} \chi_1 \\ \mu \left( \frac{\mathcal{A}\chi}{\alpha_h} \right)^{\alpha/2} \\ \left( \frac{\mathcal{C}\chi_2}{\alpha_h} \right) \end{array} \middle| \begin{array}{l} \nu_6 : \nu_7; \nu_2; \nu_3 \\ - : \nu_8; \nu_4; \nu_5 \end{array} \right]. \end{aligned} \quad (38)$$

3) *M*-ary NCFSK scheme: For any modulation scheme, the ASER expression can be evaluated by using the PDF-based approach [45] as

$$\mathcal{P}_s(e) = \int_{\lambda=0}^{\infty} \mathcal{P}_s(e|\lambda) f_{\lambda_e}(\lambda) d\lambda, \quad (40)$$

where  $f_{\lambda_e}(\lambda)$  is the PDF expression for end-to-end SNR,  $\lambda_e$ , of the considered system. The conditional SER for *M*-ary NCFSK modulation scheme can be written [45, eq. (8.67)] as

$$\mathcal{P}_s^{NC}(e|\lambda) = \sum_{\eta=1}^{M-1} \frac{(-1)^{\eta+1}}{\eta+1} \binom{M-1}{\eta} e^{-\left(\frac{\eta\lambda}{\eta+1}\right)}. \quad (41)$$

By putting (41) into (40), the ASER expression of *M*-ary NCFSK scheme can be expressed as

$$P_e^{NC} = \sum_{\eta=1}^{M-1} \frac{(-1)^{\eta+1}}{\eta+1} \binom{M-1}{\eta} \int_{\lambda=0}^{\infty} e^{-\left(\frac{\eta\lambda}{\eta+1}\right)} f_{\lambda_e}(\lambda) d\lambda. \quad (42)$$

Further, with the aid of PDF based approach of MGF calculation [45, eq. (2.4)], the ASER expression of *M*-ary NCFSK scheme can be evaluated in terms of the MGF as

$$P_e^{NC} = \sum_{\eta=1}^{M-1} \frac{(-1)^{\eta+1}}{\eta+1} \binom{M-1}{\eta} \mathcal{M}_{\lambda_e} \left( \frac{\eta}{\eta+1} \right). \quad (43)$$

Further, by substituting (26) into (43) and putting  $M = 2$ , we can write the simplified ABER expression for binary NCFSK as

$$\mathcal{P}_e^{NC} = \frac{1}{2} - \frac{\mathcal{B}}{2} H_{1,0:2,3;1,2}^{0,1:3,0;2,0} \left[ \begin{array}{c} \mu \left( \sqrt{2\mathcal{A}} \right)^{\alpha} \\ 2\mathcal{C} \end{array} \middle| \begin{array}{l} \nu_{\mathcal{M}} : \nu_2; \nu_3 \\ - : \nu_4; \nu_5 \end{array} \right]. \quad (44)$$

#### D. Asymptotic ASER Expression and Diversity Order

In order to observe the behavior of ASER in high SNR regime and to examine the system's diversity, we need to derive the asymptotic ASER for the RQAM scheme. To do so, first, we have to obtain the asymptotic expression of (19) and (20) by considering  $\bar{\lambda}_0 \rightarrow \infty$  or  $P_s \rightarrow \infty$ . In this context, we approximate the Meijer-G function of (19) with the aid of [46, eq. (07.34.06.0001.01)] as represented in (45).

$$F_{\lambda_1}^{\infty}(\lambda) \approx \frac{\Gamma\left(\mu - \frac{\phi}{\alpha}\right)}{\Gamma(\mu)} \mu^{\frac{\phi}{\alpha}} (\mathcal{A}\lambda)^{\frac{\phi}{\alpha}} + \frac{\phi \mu^{\mu} (\mathcal{A}\lambda)^{\frac{\alpha\mu}{2}}}{(\phi - \alpha\mu)\Gamma(\mu+1)}. \quad (45)$$

Further, we substitute the upper incomplete gamma function by its approximation as  $\lim_{x \rightarrow 0} \Gamma(a, x) \approx \Gamma(a) - \frac{x^a}{a}$  [40, eq. (8.354.2)] to express the asymptotic form of (20) as mentioned in (46).

$$F_{\lambda_2}^{\infty}(\lambda) \approx \frac{(\mathcal{C}\lambda)^m}{\Gamma(m+1)}. \quad (46)$$

Furthermore, the asymptotic CDF expression of  $\lambda_e$  can be approximated for DF relaying scheme as  $F_{\lambda_e}^{\infty}(\lambda) \approx F_{\lambda_1}^{\infty}(\lambda) + F_{\lambda_2}^{\infty}(\lambda)$ .  $F_{\lambda_e}^{\infty}(\lambda)$  can be obtained by adding (45) and (46) after putting the values of  $\mathcal{A}$  and  $\mathcal{C}$ , respectively, as expressed in (47), given at the next page.

1) *Asymptotic ASER for RQAM scheme*: Asymptotic ASER expression of RQAM scheme (49) can be evaluated by putting the approximated CDF of end-to-end SNR (47) and (29) into

$$\mathcal{P}_s^H(e) = \frac{B}{2} - \frac{B_c}{3} - \frac{\mathcal{B}}{\sqrt{\pi}} \left\{ \left( \frac{B_c - B}{2} \right) \Psi_3(2) - \frac{B_c}{3} \Psi_3(3) + \frac{B_c}{2} \Psi_3(6) \right\} + \frac{\mathcal{B}B_c}{\pi} \left\{ \frac{\Psi_4(1,3)}{3} - \frac{\sqrt{3}\Psi_4(3,6)}{2} - \frac{\Psi_4\left(\frac{1}{3},2\right)}{2\sqrt{3}} \right\} \quad (39)$$

$$F_{\lambda_e}^\infty(\lambda) \approx \left[ \frac{\phi\mu^\mu}{(\phi - \alpha\mu)\Gamma(\mu + 1)} \left( \frac{\lambda}{\Omega^2 S_0^2 |h_{d1}|^2 |h_{a1}|^2} \right)^{\frac{\alpha\mu}{2}} \right] \left( \frac{N_1}{P_s} \right)^{\frac{\alpha\mu}{2}} + \left[ \frac{\mu\left(\frac{\phi}{\alpha}\right)\Gamma\left(\mu - \frac{\phi}{\alpha}\right)}{\Gamma(\mu)} \left( \frac{\lambda}{\Omega^2 S_0^2 |h_{d1}|^2 |h_{a1}|^2} \right)^{\frac{\phi}{2}} \right] \left( \frac{N_1}{P_s} \right)^{\frac{\phi}{2}} + \left[ \frac{1}{\Gamma(m+1)} \left( \frac{m\lambda}{\Omega_m |h_{d2}|^2} \right)^m \right] \left( \frac{N_2}{P_r} \right)^m. \quad (47)$$

(27) as

$$\begin{aligned} \mathcal{P}_s^{R\infty}(e) = & -\mathcal{DRI}_1\left(\frac{\alpha\mu - 1}{2}, \frac{a^2}{2}\right) - \mathcal{DTI}_1\left(\frac{\phi - 1}{2}, \frac{a^2}{2}\right) \\ & - \frac{\mathcal{C}^m}{\Gamma(m+1)} \left\{ \mathcal{DI}_1\left(m - \frac{1}{2}, \frac{a^2}{2}\right) + \mathcal{FI}_1\left(m - \frac{1}{2}, \frac{b^2}{2}\right) \right\} \\ & - \mathcal{FRI}_1\left(\frac{\alpha\mu - 1}{2}, \frac{b^2}{2}\right) - \mathcal{FTI}_1\left(\frac{\phi - 1}{2}, \frac{b^2}{2}\right) \\ & + \frac{\mathcal{G}}{\sqrt{\pi}} \left[ \mathcal{RI}_3\left(\frac{\alpha\mu}{2}, \frac{a^2 + b^2}{2}, \frac{a^2}{2}\right) + \mathcal{TI}_3\left(\frac{\phi}{2}, \frac{a^2 + b^2}{2}, \frac{a^2}{2}\right) \right. \\ & + \mathcal{RI}_3\left(\frac{\alpha\mu}{2}, \frac{a^2 + b^2}{2}, \frac{b^2}{2}\right) + \mathcal{TI}_3\left(\frac{\phi}{2}, \frac{a^2 + b^2}{2}, \frac{b^2}{2}\right) \\ & + \frac{\mathcal{C}^m}{\Gamma(m+1)} \left\{ \mathcal{I}_3\left(m, \frac{a^2 + b^2}{2}, \frac{a^2}{2}\right) \right. \\ & \left. \left. + \mathcal{I}_3\left(m, \frac{a^2 + b^2}{2}, \frac{b^2}{2}\right) \right\} \right], \quad (48) \end{aligned}$$

where  $\mathcal{R} = \frac{\phi\mu^\mu}{(\phi - \alpha\mu)\Gamma(\mu+1)} \mathcal{A}^{\frac{\alpha\mu}{2}}$ ,  $\mathcal{T} = \frac{\mu^{(\phi/\alpha)}}{\Gamma(\mu)} \Gamma\left(\mu - \frac{\phi}{\alpha}\right) \mathcal{A}^{\frac{\phi}{2}}$ . Now, by substituting the integral values in (48), asymptotic ASER expression of RQAM scheme can be written in terms of  $\Psi^\infty(\cdot, \cdot)$  as represented in (49), where  $\Psi^\infty(\cdot, \cdot)$  can be written as  $\Psi^\infty(\chi_1, \chi_2) = \left(\frac{\chi_2}{2}\right)^{-\frac{\chi_1+1}{2}} \Gamma\left(\frac{\chi_1+1}{2}\right)$ .

2) *Diversity Order*: Mathematically, the diversity order can be evaluated in high SNR regime as [47]

$$\text{Diversity Order} = \lim_{\lambda_0 \rightarrow \infty} \frac{-\log P_s^\infty(e)}{\log \lambda_0}. \quad (50)$$

Thus, one can obtain the diversity order of the proposed system by putting the values of  $\mathcal{A}$  and  $\mathcal{C}$  in (49) and substituting resulting expression into (50), which can be expressed as

$$\text{Diversity Order} = \min \left\{ \frac{\alpha\mu}{2}, \frac{\phi}{2}, m \right\}. \quad (51)$$

#### IV. NUMERICAL AND SIMULATION RESULTS

In this section, we analyze the analytical, simulation and asymptotic results to understand the performance of relay-assisted THz-RF systems. We choose  $10^8$  realizations of channel coefficients and symbols in our Monte Carlo simulations to validate the theoretically generated results whereas asymptotic behavior is also observed. We consider environmental conditions such as atmospheric pressure, absolute temperature, and

relative humidity for THz link as well as different channel parameters as mentioned in Table I.

TABLE I  
LIST OF SIMULATION PARAMETERS

Parameter	Value
THz carrier frequency ( $f_{sr}$ )	275 GHz
RF carrier frequency ( $f_{rd}$ )	8 GHz
THz link Antenna Gain ( $G_{ts}, G_{rr}$ )	52 dBi
RF link Antenna Gain ( $G_{tr}, G_{rd}$ )	52 dBi
Source to Relay distance ( $d_{sr}$ )	300 Meters
Relay to Destination distance ( $d_{rd}$ )	800 Meters
Absolute Temperature ( $T$ )	296 K
Atmospheric Pressure ( $P$ )	1013.25 hPa
Relative Humidity ( $\psi$ )	50 %
THz link fading parameter ( $\alpha$ )	1.6-3.0
Normalised variance of THz link envelope ( $\mu$ )	1-3.5
$\alpha$ -root mean value of THz link envelope ( $\Omega$ )	1-2.5
Pointing Error Parameter ( $\phi$ )	1.5-12
Fraction of power collected at center ( $S_0$ )	0.39-0.73
RF link Shape Parameter ( $m$ )	1.6-3.0
RF link Spread Parameter ( $\Omega_m$ )	0.015-3.00

Fig. 2 illustrates the ASER performance of  $4 \times 2$ -RQAM scheme versus average transmit SNR for several sets of  $\alpha$  and  $\mu$ . From the figure, we find that the theoretical and simulation results match well to each other which validates the correctness of the derived expression (34). The asymptotic results also align with the theoretical and the simulation results at high SNR regime by which we can further validate the correctness of the derived expression. It is also observed that by increasing  $\alpha$  and  $\mu$ , the ASER performance improves as expected. For example, approximately 4.46 dB and 7.65 dB less SNR is required to maintain the ASER at  $6.66 \times 10^{-6}$  when  $\alpha$  is increased from 1.7 to 2 and 1.7 to 2.3, respectively, keeping other parameters constant. Similarly, when  $\mu$  is increased from 2.0 to 2.2 and 2.0 to 2.6, approximately, 1.88 dB and 3.93 dB less SNR is required, respectively, to maintain the ASER at  $3 \times 10^{-8}$ .

In Fig. 3, the ASER performance is analyzed for 8-HQAM scheme against average transmit SNR in order to demonstrate the impact of pointing error coefficients. Further, it can be observed that the theoretical results match well with the simulation results for all the investigated cases. From the figure, we perceive that the ASER performance is improved

$$\begin{aligned} \mathcal{P}_s^{R\infty}(e) = & -\mathcal{R} \left[ \mathcal{D}\Psi^\infty(\alpha\mu, a^2) - \mathcal{F}\Psi^\infty(\alpha\mu, b^2) \right] + \frac{\mathcal{G}}{\sqrt{\pi}} \left[ {}_2F_1 \left( 1, 1; \frac{3}{2}; \frac{a^2}{a^2 + b^2} \right) + {}_2F_1 \left( 1, 1; \frac{3}{2}; \frac{b^2}{a^2 + b^2} \right) \right] \times \\ & \left[ \mathcal{R}\Psi^\infty(\alpha\mu + 1, a^2 + b^2) + \mathcal{T}\Psi^\infty(\phi + 1, a^2 + b^2) + \frac{1}{\mathcal{C}} \left( \frac{2\mathcal{C}}{a^2 + b^2} \right)^{m+1} \right] - \frac{\mathcal{C}^m}{\Gamma(m+1)} \left[ \mathcal{D}\Psi^\infty(2m, a^2) + \mathcal{F}\Psi^\infty(2m, b^2) \right] \\ & - \mathcal{T} \left[ \mathcal{D}\Psi^\infty(\phi, a^2) - \mathcal{F}\Psi^\infty(\phi, b^2) \right]. \end{aligned} \quad (49)$$

with an increase in both the parameters  $\phi$  and  $S_0$ . For example, when  $\phi$  is increased from 3.62 to 4.46 and 3.62 to 5.64, approximately 3.05 dB and 4.75 dB less SNR is required, respectively, to achieve the ASER of  $1.3 \times 10^{-6}$ . Similarly, when  $S_0$  is increased from 0.61 to 0.66 and 0.61 to 0.73, approximately, 0.71 dB and 1.6 dB less SNR is required, respectively, to maintain the ASER of  $10^{-7}$  keeping all other parameters constant.

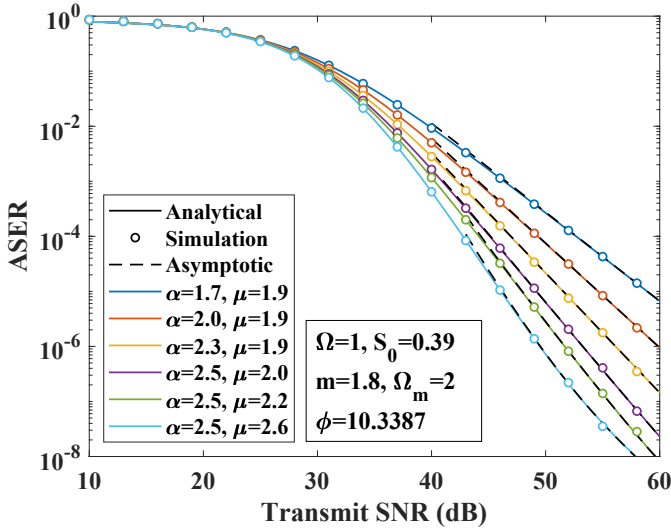


Fig. 2. ASER performance of  $4 \times 2$ -RQAM scheme versus average SNR.

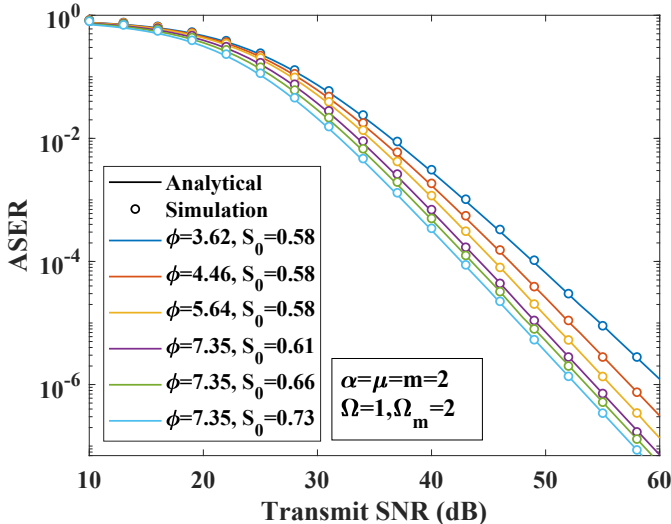


Fig. 3. ASER performance of 8-HQAM scheme against average SNR.

In Fig. 4, the ASER performance for several modulation schemes are compared. We observe that, due to the compact packing of constellation points, HQAM has the best performance among all QAM schemes. SQAM is a compact arrangement of RQAM and thus SQAM provides significantly better performance than RQAM. It is noticeable that 64-HQAM and 16-HQAM show better ASER performance than 64-SQAM and 16-SQAM respectively, though the difference in performance is very less because of their compact constellations. For example, when the modulation scheme is changed from  $8 \times 4$ -RQAM to 32-HQAM, approximately, 1.33 dB less SNR is required to maintain the ASER at  $10^{-7}$ . Also, ASER performance gets better when modulation order is reduced. From the figure, we can further observe that the higher-order modulation schemes suit perfectly for good channel conditions with high SNR at the receiver, and therefore we get the highest possible data rates without degrading the error performance much. Although, for a low SNR regime, it is better to use lower-order modulation schemes to combat severe degradation in ASER.

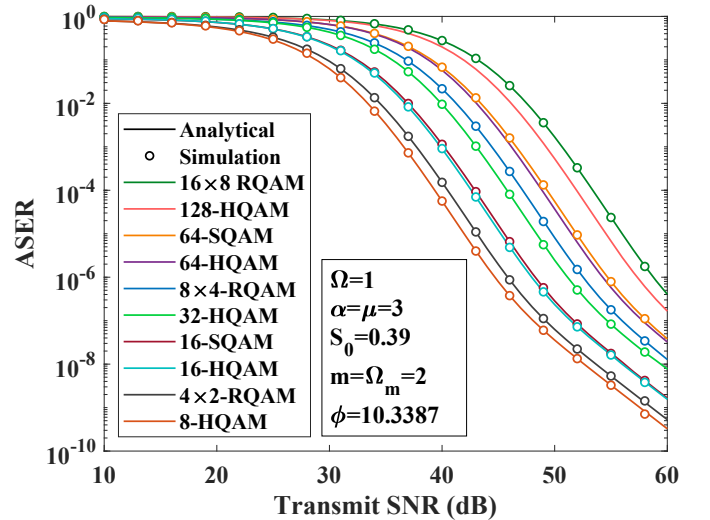


Fig. 4. Comparison of ASER performances against average SNR for several QAM constellations.

Fig. 5 shows the theoretical and the simulation results of ASER performance with respect to average transmit SNR for 2-ary NCFSK modulation scheme considering several values of RF link parameters,  $m$ , and  $\Omega_m$ , with fixed THz link parameters. From the figure, it can be seen that all the theoretical curves match well with the simulation curves for all the investigated cases. Further, it is also observed that with



the increase in  $m$  and  $\Omega_m$ , the ASER performance improves. For example, when  $m$  is increased from 1.6 to 1.8 and 1.6 to 2.1, approximately, 2.73 dB and 5.77 dB less SNR is required, respectively, to achieve the ASER of  $1.1 \times 10^{-5}$  keeping all the other parameters constant. Similarly, when  $\Omega_m$  is increased from 0.015 to 0.025 and 0.015 to 0.04, approximately, 2.23 dB and 4.27 dB of less SNR is required to maintain the ASER at  $10^{-7}$ .

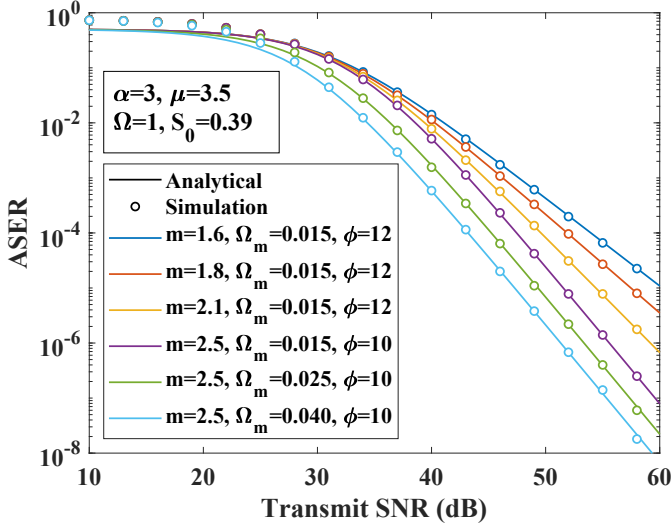


Fig. 5. ASER performance of 2-ary NCFSK modulation scheme against average SNR.

In Fig. 6, we show the impact of  $\Omega_m$  on ASER performance of  $4 \times 2$ -RQAM schemes, considering several values of  $\alpha$ ,  $\mu$  and  $\phi$  at fixed average transmit SNR and other parameters. From the figure, it can be observed that all the theoretical and simulation curves match well for all the investigated cases. It is also noticed that with the increase in  $\Omega_m$  the ASER performance improves and gets saturated further.

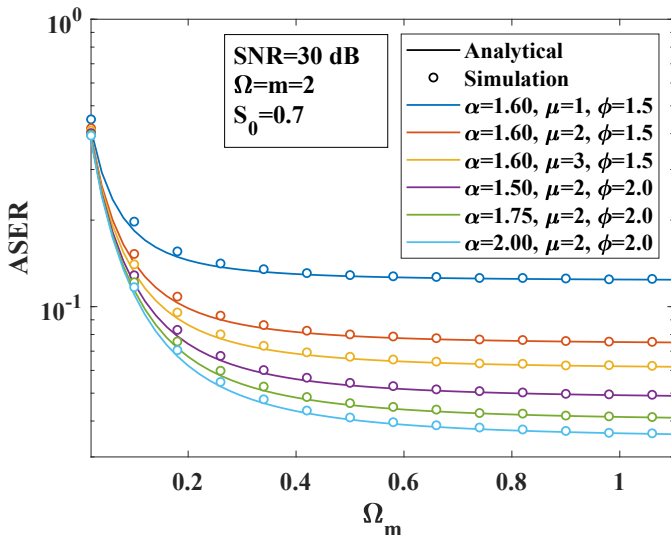


Fig. 6. ASER performance of  $4 \times 2$ -RQAM scheme against  $\Omega_m$ .

Fig. 7 represents the impact of  $d_{SR}$  on ASER performance of  $4 \times 2$ -RQAM scheme considering several values

of  $\alpha$  and  $\mu$  at fixed average transmit SNR. We consider  $d_{SR} + d_{RD} = 1100$  (meters). At fixed  $d_{SR}$ , it is computed as  $d_{RD} = 1100 - d_{SR}$ . Further, we can observe that by increasing  $d_{SR}$ , the probability of ASER increases, gets its maximum value and then decreases. From this observation, it can be depicted that the ASER performance improves when relay is near to source or destination node.

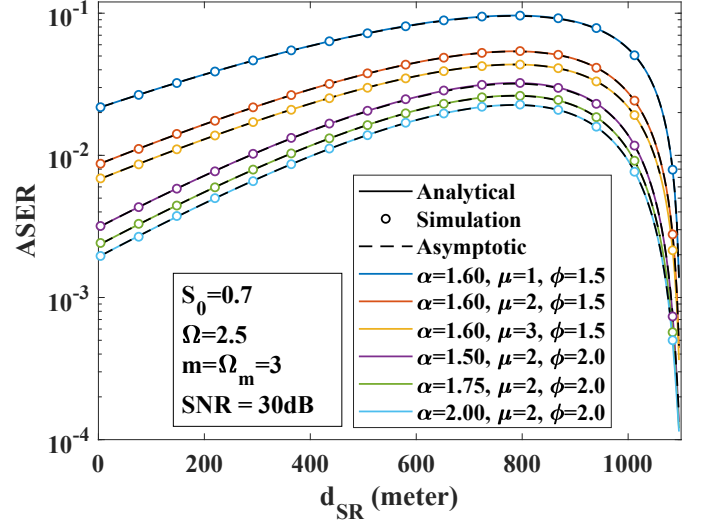


Fig. 7. ASER performance of  $4 \times 2$ -RQAM scheme against  $d_{SR}$ .

## V. CONCLUSION

In this paper, the dual-hop mixed THz-RF cooperative relay networks have been studied. The novel closed-form expressions of the CDF and MGF for the end-to-end SNR of the considered system are derived. Further, using a well-known CDF-based approach, new closed-form expressions of generalized ASER for coherent RQAM and HQAM schemes are evaluated. The asymptotic ASER expression for RQAM scheme is also provided. Using MGF, the ASER expression of the NCFSK modulation scheme is also analyzed for the considered system. Furthermore, the impact of all considered parameters of the system is highlighted on the system's performance. All the derived expressions are validated through Monte Carlo simulation results.

## APPENDIX

This appendix elaborates on the solutions of necessary integrals required to calculate ASER for RQAM (34), ASER for HQAM (39) and asymptotic ASER for RQAM (49).

### A. Calculation of (9) from (6) and (7)

With the aid of [40], CDF of THz link  $F_{h_1}(x)$  can be calculated as,

$$F_{h_1}(x) = \int_{y=0}^{S_0} F_{h_{f1}}\left(\frac{x}{y}\right) f_{h_{p1}}(y) dy. \quad (52)$$

By putting the values of  $F_{h_{f1}}(x)$  and  $f_{h_{p1}}(x)$  into (52) from (6) and (7), respectively,  $F_{h_1}(x)$  can be expressed as,

$$F_{h_1}(x) = 1 - \frac{1}{\Gamma(\mu)} \frac{\phi}{S_0^\phi} \int_{y=0}^{S_0} y^{\phi-1} \Gamma\left(\mu, \frac{\mu x^\alpha}{\Omega^\alpha y^\alpha}\right) dy. \quad (53)$$

Further, with the aid of [48], the  $\Gamma(\cdot, \cdot)$  can be written in term of Meijer G function as in (54)

$$F_{h_1}(x) = 1 - \frac{1}{\Gamma(\mu)} \frac{\phi}{S_0^\phi} \int_{y=0}^{S_0} y^{\phi-1} G_{1,2}^{2,0} \left[ \frac{\mu x^\alpha}{\Omega^\alpha y^\alpha} \middle| \begin{matrix} 1 \\ \mu, 0 \end{matrix} \right] dy. \quad (54)$$

With the aid of [34, eq. (9.301)], the Meijer G function in (54) can be written as,

$$F_{h_1}(x) = 1 - \frac{1}{\Gamma(\mu)} \frac{\phi}{S_0^\phi} \int_{y=0}^{S_0} \left( \frac{1}{2\pi i} \right) \int_s \left( \frac{\mu x^\alpha}{\Omega^\alpha S_0^\alpha} \right)^{-s} \times \frac{\Gamma(\mu+s)\Gamma(s)}{\Gamma(1+s)} \int_{y=0}^{S_0} y^{\phi+\alpha s-1} dy ds \quad (55)$$

After solving the inner integral, (55) can be written in term of a Meijer G function with the aid of [34, eq. (9.301)], as expressed in (9).

$$F_{h_1}(x) = 1 - \frac{1}{\Gamma(\mu)} \frac{\phi}{\alpha} G_{2,3}^{3,0} \left[ \frac{\mu x^\alpha}{\Omega^\alpha S_0^\alpha} \middle| \begin{matrix} 1, \frac{\phi}{\alpha} + 1 \\ \mu, 0, \frac{\phi}{\alpha} \end{matrix} \right]. \quad (56)$$

### B. A Solution of $\mathcal{I}_1(\chi_1, \chi_2)$

The integration part in (24) can be written with respect to  $(\chi_2 \lambda)$  as

$$\mathcal{I}_1(\chi_1, \chi_2) = \int_{\chi_2 \lambda=0}^{\infty} (\chi_2 \lambda)^{\chi_1} e^{-\chi_2 \lambda} \left( \frac{1}{\chi_2} \right)^{(\chi_1+1)} d(\chi_2 \lambda). \quad (57)$$

From the definition of gamma function [34, eq. (8.310.1)], (57) can be written as

$$\mathcal{I}_1(\chi_1, \chi_2) = \left( \frac{1}{\chi_2} \right)^{\chi_1+1} \Gamma(\chi_1 + 1). \quad (58)$$

### C. A Solution of $\mathcal{I}_2(\chi_1, \chi_2)$

Substituting the Meijer-G representation of  $\Gamma(m, \mathcal{C}\lambda)$  with the aid of [48],  $\mathcal{I}_2(\cdot, \cdot)$  can be written as

$$\mathcal{I}_2(\chi_1, \chi_2) = \int_{\lambda=0}^{\infty} \frac{\lambda^{\chi_1}}{e^{\lambda_2 \lambda}} G_{1,2}^{2,0} \left[ \mathcal{C}\lambda \middle| \begin{matrix} 1 \\ m, 0 \end{matrix} \right] \times G_{2,3}^{3,0} \left[ \mu (\mathcal{A}\lambda)^{\alpha/2} \middle| \begin{matrix} 1, \frac{\phi}{\alpha} + 1 \\ \mu, 0, \frac{\phi}{\alpha} \end{matrix} \right] d\lambda. \quad (59)$$

Further, putting the equivalent integral form of meijer G functions, the overall integral in (59) can be expressed in term of  $\mathcal{I}_1(\cdot, \cdot)$  as

$$\mathcal{I}_2(\chi_1, \chi_2) = \left( \frac{1}{2\pi i} \right)^2 \int_s \int_t \varphi_2(s) \varphi_3(t) \times \mathcal{I}_1\left(\chi_1 - \frac{\alpha s}{2} - t, \chi_2\right) ds dt, \quad (60)$$

where, using  $\Gamma(\chi+1) = \chi\Gamma(\chi)$ , the functions  $\varphi_2(s)$ ,  $\varphi_3(t)$  can be expressed in simplified form as  $\varphi_2(s) =$

$\frac{\alpha\Gamma(\mu+s)}{s(\phi+\alpha s)} \left\{ \mu (\mathcal{A})^{\alpha/2} \right\}^{-s}$  and  $\varphi_3(t) = \frac{\Gamma(m+t)}{t \mathcal{C}^t}$ . Further, by putting the solution of  $\mathcal{I}_1(\cdot, \cdot)$  from (58), the  $\mathcal{I}_2(\cdot, \cdot)$  can be expressed as a bivariate fox H function with the aid of [37, eq. (A.1)] as

$$\mathcal{I}_2(\chi_1, \chi_2) = \frac{1}{\chi_2^{\chi_1+1}} H_{1,0;2,3;1,2}^{0,1;3,0;2,0} \left[ \begin{matrix} \mu \left( \sqrt{\frac{\mathcal{A}}{\chi_2}} \right)^\alpha \\ \frac{\mathcal{C}}{\chi_2} \end{matrix} \middle| \begin{matrix} \nu_1 : \nu_2; \nu_3 \\ - : \nu_4; \nu_5 \end{matrix} \right] \quad (61)$$

where,  $\nu_1(\chi_1) = \{(-\chi_1; \frac{\alpha}{2}, 1)\}$ ,  $\nu_2 = \{(1, 1), (\frac{\phi}{\alpha} + 1, 1)\}$ ,  $\nu_3 = \{(1, 1)\}$ ,  $\nu_4 = \{(\mu, 1), (\frac{\phi}{\alpha}, 1), (0, 1)\}$  and  $\nu_5 = \{(m, 1), (0, 1)\}$ .

### D. A Solution of $\mathcal{I}_3(\chi_1, \chi_2)$

The function  ${}_1F_1(\cdot; \cdot; \cdot)$  present in (30) can be expressed into its series form with the aid of [34, eq. (9.210.1)], and therefore, the  $\mathcal{I}_3(\chi_1, \chi_2, \chi_3)$  can be written as

$$\mathcal{I}_3(\chi_1, \chi_2, \chi_3) = \sum_{\eta=0}^{\infty} \frac{\Gamma(\frac{3}{2})\Gamma(\eta+1)}{\Gamma(\frac{3}{2}+\eta)} \frac{\chi_3^\eta}{\eta!} \int_{\lambda=0}^{\infty} \lambda^{\eta+\chi_1} e^{-\chi_2 \lambda} d\lambda. \quad (62)$$

The integration part in (62) is similar to  $\mathcal{I}_1(\cdot, \cdot)$  and thus can be solved by using (58) as

$$\begin{aligned} \mathcal{I}_3(\chi_1, \chi_2, \chi_3) &= \sum_{\eta=0}^{\infty} \frac{\Gamma(\frac{3}{2})\Gamma(\eta+1)}{\Gamma(\frac{3}{2}+\eta)} \frac{\chi_3^\eta}{\eta!} \mathcal{I}_1(\eta+\chi_1, \chi_2) \\ &= \frac{\Gamma(\chi_1+1)}{\chi_2^{\chi_1+1}} \sum_{\eta=0}^{\infty} \frac{\Gamma(\eta+1)\Gamma(\frac{3}{2})\Gamma(\eta+1)}{\Gamma(\frac{3}{2}+\eta)} \frac{(\chi_3/\chi_2)^\eta}{\eta!}. \end{aligned} \quad (63)$$

Further, with the aid of [35, eq. (7.2.3)], the  $\mathcal{I}_3(\chi_1, \chi_2, \chi_3)$  can be written in term of hypergeometric function as

$$\mathcal{I}_3(\chi_1, \chi_2, \chi_3) = \frac{\Gamma(\chi_1+1)}{\chi_2^{\chi_1+1}} {}_2F_1\left(1, 1; \frac{3}{2}; \frac{\chi_3}{\chi_2}\right). \quad (64)$$

### E. A Solution of $\mathcal{I}_4(\chi_1, \chi_2)$

The function  ${}_1F_1(\cdot; \cdot; \cdot)$  and  $\Gamma(\cdot, \cdot)$  present in (31) can be expressed into their equivalent meijer G representation with the aid of [49] and [48] respectively as

$$\begin{aligned} \mathcal{I}_4(\chi_1, \chi_2) &= \frac{1}{2} \int_{\lambda=0}^{\infty} e^{-(\chi_1-\chi_2)\lambda} G_{1,2}^{1,1} \left[ \chi_2 \lambda \middle| \begin{matrix} 1 \\ 0, -\frac{1}{2} \end{matrix} \right] \\ &\times G_{2,3}^{3,0} \left[ \mu (\mathcal{A}\lambda)^{\alpha/2} \middle| \begin{matrix} 1, \frac{\phi}{\alpha} + 1 \\ \mu, 0, \frac{\phi}{\alpha} \end{matrix} \right] G_{1,2}^{2,0} \left[ \mathcal{C}\lambda \middle| \begin{matrix} 1 \\ m, 0 \end{matrix} \right] d\lambda. \end{aligned} \quad (65)$$

Further, with the aid of [Definition of Meijer G], meijer G functions in (65) can be expressed with their equivalent integral form. Thus, after performing some simplifications

using  $\Gamma(\chi + 1) = \chi\Gamma(\chi)$ , the overall integral can be written in term of  $\mathcal{I}_1(\cdot, \cdot)$  as

$$\mathcal{I}_4(\chi_1, \chi_2) = \left(\frac{1}{2\pi i}\right)^3 \int_r \int_s \int_t \varphi_1(r) \varphi_2(s) \varphi_3(t) \times \mathcal{I}_1\left(-r - \frac{\alpha s}{2} - t, \chi_1 - \chi_2\right) dr ds dt, \quad (66)$$

where,  $\varphi_1(r) = \frac{\Gamma(r)}{(1-2r)\chi_2^r}$ . After solving the integral  $\mathcal{I}_1(\cdot, \cdot)$ , equation (66) can be written as

$$\mathcal{I}_4(\chi_1, \chi_2) = \left(\frac{1}{2\pi i}\right)^3 \int_r \int_s \int_t \varphi_1(r) \varphi_2(s) \varphi_3(t) \times \frac{\Gamma\left(1 - r - \frac{\alpha s}{2} - t\right)}{(\chi_1 - \chi_2)^{1-r-(\alpha s/2)-t}} dr ds dt. \quad (67)$$

Further, with the aid of [37, eq. (A.1)], equation (67) can be written in term of trivariate fox H as

$$\mathcal{I}_4(\chi_1, \chi_2) = \frac{1}{2(\chi_1 - \chi_2)} \times H_{1,0:1,2;2,3;1,2}^{0,1:1,0;3,0;2,0} \left[ \begin{array}{c} \left(\frac{\chi_2}{\chi_1 - \chi_2}\right) \\ \mu \left(\frac{A}{\chi_1 - \chi_2}\right)^{\alpha/2} \\ \left(\frac{C}{\chi_1 - \chi_2}\right) \end{array} \middle| \begin{array}{l} \nu_6 : \nu_7; \nu_2; \nu_3 \\ - : \nu_8; \nu_4; \nu_5 \end{array} \right], \quad (68)$$

where,  $\nu_6 = \left\{\left(0; 1, \frac{\alpha}{2}, 1\right)\right\}$ ,  $\nu_7 = \left\{\left(\frac{1}{2}, 1\right)\right\}$  and  $\nu_8 = \left\{\left(0, 1\right), \left(-\frac{1}{2}\right)\right\}$ .

## REFERENCES

- [1] H. Elayan, O. Amin, B. Shihada, R. M. Shubair, and M.-S. Alouini, "Terahertz Band: The Last Piece of RF Spectrum Puzzle for Communication Systems," *IEEE Open Journal of the Communications Society*, vol. 1, pp. 1–32, 2020.
- [2] A.-A. A. Boulogeorgos, A. Alexiou, T. Merkle, C. Schubert, R. Elschner, A. Katsiotis, P. Stavrianos, D. Kritharidis, P.-K. Chartsias, J. Kokkonemi, M. Juntti, J. Lehtomaki, A. Teixeira, and F. Rodrigues, "Terahertz Technologies to Deliver Optical Network Quality of Experience in Wireless Systems Beyond 5G," *IEEE Communications Magazine*, vol. 56, no. 6, pp. 144–151, 2018.
- [3] I. F. Akyildiz, J. M. Jornet, and C. Han, "Terahertz band: Next frontier for wireless communications," *Physical Communication*, vol. 12, pp. 16–32, 2014.
- [4] C. Zhang, K. Ota, J. Jia, and M. Dong, "Breaking the Blockage for Big Data Transmission: Gigabit Road Communication in Autonomous Vehicles," *IEEE Communications Magazine*, vol. 56, no. 6, pp. 152–157, 2018.
- [5] V. Petrov, A. Pyattaev, D. Moltchanov, and Y. Koucheryavy, "Terahertz band communications: Applications, research challenges, and standardization activities," in *2016 8th International Congress on Ultra Modern Telecommunications and Control Systems and Workshops (ICUMT)*, 2016, pp. 183–190.
- [6] G. A. Siles, J. M. Riera, and P. Garcia-del Pino, "Atmospheric Attenuation in Wireless Communication Systems at Millimeter and THz Frequencies [Wireless Corner]," *IEEE Antennas and Propagation Magazine*, vol. 57, no. 1, pp. 48–61, 2015.
- [7] C. Han and Y. Chen, "Propagation Modeling for Wireless Communications in the Terahertz Band," *IEEE Communications Magazine*, vol. 56, no. 6, pp. 96–101.
- [8] M. D. Yacoub, "The  $\alpha$ - $\mu$  Distribution: A Physical Fading Model for the Stacy Distribution," *IEEE Transactions on Vehicular Technology*, vol. 56, no. 1, pp. 27–34, 2007.
- [9] J. M. Jornet and I. F. Akyildiz, "Channel Modeling and Capacity Analysis for Electromagnetic Wireless Nanonetworks in the Terahertz Band," *IEEE Transactions on Wireless Communications*, vol. 10, no. 10, pp. 3211–3221, 2011.
- [10] J. Kokkonemi, J. Lehtomki, and M. Juntti, "Simplified molecular absorption loss model for 275400 gigahertz frequency band," in *12th European Conference on Antennas and Propagation (EuCAP 2018)*, 2018, pp. 1–5.
- [11] A.-A. A. Boulogeorgos, E. N. Pappasotiriou, J. Kokkonemi, J. Lehtomaki, A. Alexiou, and M. Juntti, "Performance Evaluation of THz Wireless Systems Operating in 275–400 GHz Band," in *2018 IEEE 87th Vehicular Technology Conference (VTC Spring)*, 2018, pp. 1–5.
- [12] M. A. Akkas, "Terahertz channel modelling of wireless ultra-compact sensor networks using electromagnetic waves," *IET Communications*, vol. 10, no. 13, pp. 1665–1672, 2016.
- [13] C. Han, A. O. Bicen, and I. F. Akyildiz, "Multi-Ray Channel Modeling and Wideband Characterization for Wireless Communications in the Terahertz Band," *IEEE Transactions on Wireless Communications*, vol. 14, no. 5, pp. 2402–2412, 2015.
- [14] A.-A. A. Boulogeorgos and A. Alexiou, "Error Analysis of Mixed THz-RF Wireless Systems," *IEEE Communications Letters*, vol. 24, no. 2, pp. 277–281, 2020.
- [15] S. Priebe, M. Jacob, and T. Krner, "The impact of antenna directivities on THz indoor channel characteristics," in *2012 6th European Conference on Antennas and Propagation (EUCAP)*, 2012, pp. 478–482.
- [16] C. Han and I. F. Akyildiz, "Three-Dimensional End-to-End Modeling and Analysis for Graphene-Enabled Terahertz Band Communications," *IEEE Transactions on Vehicular Technology*, vol. 66, no. 7, pp. 5626–5634, 2017.
- [17] A.-A. A. Boulogeorgos, E. N. Pappasotiriou, and A. Alexiou, "Analytical Performance Assessment of THz Wireless Systems," *IEEE Access*, vol. 7, pp. 11 436–11 453, 2019.
- [18] A. R. Ekti, A. Boyaci, A. Alparslan, S. Yarkan, A. Grin, H. Arslan, and M. Uysal, "Statistical modeling of propagation channels for Terahertz band," in *2017 IEEE Conference on Standards for Communications and Networking (CSCN)*, 2017, pp. 275–280.
- [19] S. Priebe, C. Jastrow, M. Jacob, T. Kleine-Ostmann, T. Schrader, and T. Krner, "Channel and Propagation Measurements at 300 GHz," *IEEE Transactions on Antennas and Propagation*, vol. 59, no. 5, pp. 1688–1698, 2011.
- [20] V. U. Pai, P. Bhardwaj, and S. M. Zafaruddin, "Performance Analysis of Dual-Hop THz Wireless Transmission for Backhaul Applications," in *2021 IEEE International Conference on Advanced Networks and Telecommunications Systems (ANTS)*, 2021, pp. 438–443.
- [21] P. Bhardwaj and S. M. Zafaruddin, "Performance of Dual-Hop Relaying for THz-RF Wireless Link," in *2021 IEEE 93rd Vehicular Technology Conference (VTC2021-Spring)*, 2021, pp. 1–5.
- [22] P. Bhardwaj and S. M. Zafaruddin, "On the Performance of Multihop THz Wireless System Over Mixed Channel Fading with Shadowing and Antenna Misalignment," *IEEE Transactions on Communications*, pp. 1–1, 2022.
- [23] E. Bjornson, M. Matthaiou, and M. Debbah, "A New Look at Dual-Hop Relaying: Performance Limits with Hardware Impairments," *IEEE Transactions on Communications*, vol. 61, no. 11, pp. 4512–4525, 2013.
- [24] P. Bhardwaj and S. Zafaruddin, "Performance of Dual-Hop Relaying for THz-RF Wireless Link Over Asymmetrical  $\alpha$ - $\mu$  Fading," *IEEE Transactions on Vehicular Technology*, vol. 70, no. 10, pp. 10031–10047, 2021.
- [25] N. Beaulieu, "A useful integral for wireless communication theory and its application to rectangular signaling constellation error rates," *IEEE Transactions on Communications*, vol. 54, no. 5, pp. 802–805, 2006.
- [26] L. Rugini, "Symbol Error Probability of Hexagonal QAM," *IEEE Communications Letters*, vol. 20, no. 8, pp. 1523–1526, 2016.
- [27] D. Matos, R. Correia, H. T. P. Silva, H. S. Silva, A. S. R. Oliveira, and N. B. Carvalho, "On the Performance of Square, Rectangular, Star, and Hexagonal QAM for Backscatter Systems," *IEEE Microwave and Wireless Components Letters*, pp. 1–4, 2022.
- [28] D. Dixit, N. Kumar, and A. K. Mandpura, "On the ASER performance of SC receiver with RQAM and HQAM over  $\kappa$ - $\mu$  fading," *AEU - International Journal of Electronics and Communications*, vol. 138, pp. 153883, 2021.
- [29] D. Dixit, N. Kumar, S. Sharma, V. Bhatia, S. Panic, and C. Stefanovic, "On the ASER Performance of UAV-Based Communication Systems for QAM Schemes," *IEEE Communications Letters*, vol. 25, no. 6, pp. 1835–1838, 2021.

- [30] P. K. Singya, P. Shaik, N. Kumar, V. Bhatia, and M.-S. Alouini, "A Survey on Higher-Order QAM Constellations: Technical Challenges, Recent Advances, and Future Trends," *IEEE Open Journal of the Communications Society*, vol. 2, pp. 617–655, 2021.
- [31] T. K. Oikonomou, S. A. Tegos, D. Tyrovolas, P. D. Diamantoulakis, and G. K. Karagiannidis, "On the Error Analysis of Hexagonal-QAM Constellations," *IEEE Communications Letters*, vol. 26, no. 8, pp. 1764–1768, 2022.
- [32] R. K. Singh, N. Kumar, and D. Dixit, "On the ASER performance of RF energy harvesting multiple relay networks," *Physical Communication*, vol. 54, p. 101847, 2022.
- [33] 3GPP, "Digital cellular telecommunications system (Phase 2+) (GSM); Universal Mobile Telecommunications System (UMTS); LTE; 5G;," 3rd Generation Partnership Project (3GPP), Technical Specification (TS) 21.915, 10 2019, version 15.0.0.
- [34] I. S. Gradshteyn and I. M. Ryzhik, *Table of integrals, series, and products*. Academic press, 2014.
- [35] A. P. Prudnikov and etc., *More Special Functions*, ser. Integrals & Series. London, England: Taylor & Francis, Jan. 1990.
- [36] H. Srivastava, "A note on certain identities involving generalized hypergeometric series," *Indagationes Mathematicae (Proceedings)*, vol. 82, no. 1, pp. 191–201, 1979.
- [37] A. M. Mathai, R. K. Saxena, and H. J. Haubold, "On the H-Function With Applications". New York, NY: Springer New York, 2010, pp. 1–43.
- [38] C. A. Balanis, *Modern antenna handbook*. John Wiley & Sons, 2011.
- [39] O. A. Alduchov and R. E. Eskridge, "Improved Magnus Form Approximation of Saturation Vapor Pressure," *Journal of Applied Meteorology and Climatology*, vol. 35, no. 4, pp. 601–609, 1996.
- [40] A. Papoulis and S. Unnikrishna Pillai, *Probability, random variables and stochastic processes*, 4th ed., ser. McGraw-Hill series in electrical and computer engineering. Maidenhead, England: McGraw Hill Higher Education, Dec. 2001.
- [41] A. A. Farid and S. Hranilovic, "Outage Capacity Optimization for Free-Space Optical Links With Pointing Errors," *Journal of Lightwave Technology*, vol. 25, no. 7, pp. 1702–1710, 2007.
- [42] M. Nakagami, "The m-Distribution - A General Formula of Intensity Distribution of Rapid Fading," in *Statistical Methods in Radio Wave Propagation*, W. HOFFMAN, Ed. Pergamon, 1960, pp. 3–36.
- [43] N. Kumar, P. K. Singya, and V. Bhatia, "ASER Analysis of Hexagonal and Rectangular QAM Schemes in Multiple-Relay Networks," *IEEE Transactions on Vehicular Technology*, vol. 67, no. 2, pp. 1815–1819, 2018.
- [44] P. K. Singya, N. Kumar, V. Bhatia, and M.-S. Alouini, "On the Performance Analysis of Higher Order QAM Schemes Over Mixed RF/FSO Systems," *IEEE Transactions on Vehicular Technology*, vol. 69, no. 7, pp. 7366–7378, 2020.
- [45] M. K. Simon and M.-S. Alouini, "Digital Communications Over Fading Channels (M.K. Simon and M.S. Alouini; 2005) [Book Review]," *IEEE Transactions on Information Theory*, vol. 54, no. 7, pp. 3369–3370, 2008.
- [46] "Meijer G-function: Series representations (formula 07.34.06.0001)," <https://functions.wolfram.com/07.34.06.0001.01>, [Accessed 17-Feb-2023].
- [47] Z. Wang and G. B. Giannakis, "A simple and general parameterization quantifying performance in fading channels," *IEEE Transactions on Communications*, vol. 51, no. 8, pp. 1389–1398, 2003.
- [48] "Incomplete gamma function: Representations through more general functions (formula 06.06.26.0005) — functions.wolfram.com," <http://functions.wolfram.com/06.06.26.0005.01>, [Accessed 06-Mar-2023].
- [49] "Kummer confluent hypergeometric function 1F1: Representations through more general functions (formula 07.20.26.0015) — functions.wolfram.com," <http://functions.wolfram.com/07.20.26.0015.01>, [Accessed 06-Mar-2023].